Drug Resistance Updates 84 (2026) 101318

Contents lists available at ScienceDirect

Drug Resistance Updates

journal homepage: www.elsevier.com/locate/drup

Loss of cyclin C drives resistance to anti-TIGIT therapy by upregulating CD155-mediated immune evasion

Shiyu Mao [a,b,1], Yadong Guo [a,b,1], Chengyuan Dong [a,c,1], Dongdong Wang [a,1], Xinbo Wang [a], Linjun Weng [a], Yanrong Yang [a], Yaxu Li [a], Tingting Niu [a], Qi Wu [a], Zening Zheng [a], Zezhi Shan [a,d], Xiao Tan [a], Yaohui Gao [e], Jiali Jin [a], Ping Wang [a], Xin Ge [a,*], Bing Shen [a,b,**], Xudong Yao [a,b,**], Lan Fang [a,*]

[a] Tongji University Cancer Center, Shanghai Tenth People's Hospital, Tongji University School of Medicine, Shanghai 200072, China
[b] Department of Urology, Urologic Cancer Institute, Shanghai Tenth People's Hospital, Tongji University School of Medicine, Shanghai 200072, China
[c] Medical College, Anhui University of Science and Technology, Huainan 232001, China
[d] Department of Colorectal Surgery, Fudan University Shanghai Cancer Center, Shanghai 200032, China
[e] Department of Pathology, Shanghai Tenth People's Hospital, Tongji University School of Medicine, Shanghai 200072, China

ARTICLE INFO

Keywords:
Immune checkpoint CD155
Transcriptional regulation
Ubiquitination
Immunotherapy

ABSTRACT

Aims: CD155 is an immune checkpoint protein expressed in tumor cells that interacts with its ligand T cell immunoreceptor with immunoglobulin and ITIM domain (TIGIT) on natural killer (NK) cells and T cells, mediating inhibitory regulation on immune cells. Blockade of the CD155-TIGIT interaction has demonstrated clinical benefits in patients with advanced cancers. The transcriptional and post-translational mechanisms governing CD155 expression remain largely unknown.

Methods: To identify regulators of CD155, we conducted a genome-wide CRISPR-Cas9 screen in cancer cells. Surface CD155 protein levels were analyzed via flow cytometry. The role of candidate regulators was validated through loss- and gain-of-function experiments with flow cytometry, Western blot, quantitative PCR, and chromatin immunoprecipitation (ChIP) assays. Additionally, ubiquitination assay was performed to examine post-translational modifications. Functional studies, including NK and T cell cytotoxicity assays, were conducted to assess the immune modulatory effects of CD155 regulation. Clinical relevance was evaluated by analyzing Cyclin C (CCNC) and CD155 expression in datasets of cancer patients who underwent immune checkpoint blockade therapy.

Results: The CRISPR-Cas9 screen identified CCNC as a transcriptional suppressor of CD155. *CCNC* knockout led to increased surface CD155 expression in cancer cell lines. Mechanistically, CCNC inhibited CD155 transcription by suppressing the activity of the transcription factor FOSL2. Furthermore, CCNC was found to be ubiquitinated and degraded by the E3 ubiquitin ligase FBXO11, suggesting a post-translational regulatory mechanism. Functionally, loss of CCNC promoted CD155 upregulation, thereby enhancing tumor immune evasion from NK and T cell-mediated responses. Clinically, CCNC expression was negatively correlated with CD155 levels in cancer patients, particularly those receiving immune checkpoint blockade therapy.

Conclusion: This study identifies a previously unrecognized master regulator CCNC that functions as a suppressor of CD155-mediated cancer immune evasion. The findings of this study suggest that tumors with low CCNC expression may be resistant to monotherapy and highlight a combination immunotherapy (TIGIT/PD-1 co-blockade) as a promising anti-cancer therapeutic strategy to overcome immune evasion in CCNC-deficient tumors.

* Corresponding authors.
** Corresponding authors at: Tongji University Cancer Center, Shanghai Tenth People's Hospital, Tongji University School of Medicine, Shanghai 200072, China.
E-mail addresses: xin.ge@tongji.edu.cn (X. Ge), urodrshenbing@shsmu.edu.cn (B. Shen), yaoxudong1967@163.com (X. Yao), lanfang@tongji.edu.cn (L. Fang).
[1] These authors contributed equally.

https://doi.org/10.1016/j.drup.2025.101318
Received 17 April 2025; Received in revised form 16 October 2025; Accepted 24 October 2025
Available online 10 November 2025

Introduction

Cancer cells escape destruction by the immune system through exploiting a plethora of immunosuppressive pathways (Chen and Mellman, 2017). One such escape mechanism involves the induction of inhibitory receptors on tumor-infiltrating T cells, such as programmed death receptor-1 (PD-1), cytotoxic T-lymphocyte-associated protein 4 (CTLA-4), and T cell immunoreceptor with immunoglobulin and ITIM domain (TIGIT) (Kubli et al., 2021; Freed-Pastor et al., 2021; Ribas and Wolchok, 2018). Antibody-mediated blockade of these receptors improves the outcome for cancer patients (Guan et al., 2024). Driven by the clinical success of immune checkpoint blockade (ICB), research has focused on understanding the biology and utility of immune cell inhibitory receptors (Sharma et al., 2023; Wang et al., 2024).

The poliovirus receptor (PVR, also known as CD155), a member of the nectin-like family of adhesion molecules, is frequently upregulated on tumor cells across various cancer types and has been associated with poor patient outcomes and resistance to immunotherapy (Gao et al., 2017; Pende et al., 2006). In addition to its well described cell-intrinsic roles in promoting tumor progression and metastasis, CD155 has been implicated in immune regulation through interactions with the co-stimulatory immune receptor CD226 (DNAM-1), TIGIT, and CD96, which are differentially regulated on the cell surface of T cells and natural killer (NK) cells (O'Donnell et al., 2020; Braun et al., 2020a; Shibuya et al., 1996; Martinet and Smyth, 2015; Ding et al., 2024).

The integration of signals from CD155 cognate receptors regulate the activity of tumor-infiltrating lymphocytes in a context-dependent manner, making CD155 an attractive target for immune-oncology. Preclinical studies suggest that targeting CD155 can improve immune-mediated tumor control, particularly when combined with existing anti-PD-1 checkpoint therapies (Freed-Pastor et al., 2021; Banta et al., 2022a; Yang et al., 2024; Chu et al., 2023). A phase II clinical trial CITYSCAPE on anti-TIGIT combined with anti-PD-L1 monoclonal antibody in the treatment of non-small cell lung cancer showed that, after a median follow-up of 30.4 months, treatment with tiragolumab plus atezolizumab increased the objective response rate by 18.2 % and prolonged the overall survival by 8.7 months, compared with placebo plus atezolizumab (Cho et al., 2022). The above studies show that CD155 play key roles in tumor progression and immune response. These studies emphasize the importance of understanding the regulation of CD155 in cancer cells to optimize effective targeting with immunotherapy.

Although T cels can exert potent anti-tumor immunity, a subset of T helper (Th) cells produce interleukin-22 (IL-22), which drives the expression of CD155 by cancer cells to suppress NK cell function and promote cancer metastasis (Briukhovetska et al., 2023). MicroRNA-326 negatively regulates CD155 expression at the posttranscriptional level in lung adenocarcinoma, which is one of the mechanisms of resistance to programmed death receptor-1 (PD-1)/PD-1 ligand (PD-L1) inhibitors (Nakanishi et al., 2023). However, the regulation of CD155 expression in tumor cells remains largely unknown.

Loss-of-function genetic screens have increasingly been used to study the functional consequences of gene deletion in tumor cells (Dersh et al., 2021; Burr et al., 2019; Chen et al., 2023). CD155 expression provide a survival advantage to cancer cells under immune selection pressure. Here, we use a CRISPR-Cas9 genome-wide screen to discover genes that regulate CD155 expression. This screen identified a number of genes with the potential to regulate surface CD155 protein, including *CCNC* (Li et al., 1996), which encodes cyclin C to interact with cyclin-dependent kinase 8 and induce the phosphorylation of the carboxy-terminal domain of the large subunit of RNA polymerase II (Freitas et al., 2022; Chen et al., 2021a). In this study, we show that CCNC functions as a suppressor of CD155-mediated cancer immune evasion. Loss of function of CCNC represses responses to TIGIT/PD-1 co-blockade and causes resistance to immunotherapy.

Results

Genome-wide CRISPR-Cas9 screens identify CCNC as a suppressor of cell-surface CD155

To identify conserved negative regulators of CD155 expression, we performed a fluorescence-activated cell sorting (FACS) whole genome CRISPR/Cas9 screen in DLD1 cells, a well-characterized colon cancer cell line that has intermediate level of CD155 expression (Fig. 1a). Two independent screens were performed with two different anti-human CD155 monoclonal antibodies (SKII.4 and TX24), both of which have been widely used to examine CD155. Through FACS, we separated cell populations with low and high CD155 surface expression ($CD155^{low}$ and $CD155^{high}$) (Fig. 1a). Counts of single-guide RNA (sgRNA) sequences were used to calculate gene-specific segregation scores-Z-score-based measurements of the ratio of sgRNA sequences in $CD155^{high}$ versus $CD155^{low}$ populations. STARS software was used to score genes via ranking and quantity of enriched sgRNAs in sorted populations relative to input controls. The sgRNAs targeting CD155 (PVR) were enriched and ranked the top in the $CD155^{low}$ group (Supplementary Fig. S1a, b), supporting the validity of our screen.

Here, sgRNAs identified 923 and 666 genes significantly enriched in SKII.4 and TX24 antibody group, respectively (Supplementary Table S1). Further analysis showed that 158 genes, which may negatively regulate CD155 expression, were enriched in the $CD155^{high}$ populations (Supplementary Table S1). The candidate negative regulators clustered into functional pathways that include Mediator complex, metabolism of folate and pterines, Spt–Ada–Gcn5 acetyltransferase (SAGA)-type complex, protein localization, human T-cell leukemia virus 1 infection, and Nucleotide-binding oligomerization domain-like receptor (NOD-like receptor) pathway (Supplementary Fig. S1c). Network analysis also showed that these genes were involved in Mediator complex, SAGA-type complex, mRNA metabolic process, and ornithine metabolic process (Supplementary Fig. S1d). The most significantly enriched one of these genes were single guide RNAs targeting *CCNC*, encoding core components of the Mediator kinase module, and *MED1* (Koschubs et al., 2010), serving as a surrogate of the general transcription coactivator complex for identifying active enhancers (Fig. 1b, c, and Supplementary Fig. S1e). *RNF138* and *UFM1* (Ismail et al., 2015; Komatsu et al., 2024), encoding the RING-finger E3 ubiquitin ligase (RNF138) and ubiquitin-fold modifier 1 (UFM1) that have been implicated in ubiquitination and ufmylation system, were also among the top hits (Fig. 1b, c, and Supplementary Fig. S1e). Thus, we generated *CCNC*, *MED1*, *RNF138*, and *UFM1* deficient colorectal cancer (DLD1) and bladder cancer (T24) cells using independent sgRNAs, and found that knockout of *CCNC*, *MED1*, and *RNF138* increased the cell surface expression of CD155 (Fig. 1d, e), while knockout of *UFM1* had no effect on surface CD155 expression (data not shown). Importantly, the cell surface expression of CD155 is higher in deficiency of *CCNC* than in deficiency of *MED1* and *RNF138* (Fig. 1e). CCNC is the most conserved subunit of the Mediator complex, which is an important transcription cofactor, therefore this complex was prioritized for validation. These results were further confirmed using independent sgRNAs targeting *CCNC* in bladder cancer (T24 and MB49) and colorectal cancer (DLD1 and CT26) cells (Fig. 1f-h and Supplementary Fig. S1f). These findings indicate that CCNC suppresses cell-surface CD155, and its loss promotes immune evasion and resistance to immunotherapy through CD155 overexpression.

Ccnc deficiency suppresses anti-tumor immunity through CD155/TIGIT

To examine the effects of CCNC on tumor growth, we generated *CCNC* or *Ccnc* deficient human (T24) and mouse (MB49) tumor cells. It was found that *CCNC* or *Ccnc* deficiency suppressed tumor cell proliferation and colony formation *in vitro* (Supplementary Fig. S2a-c). Notably, *Ccnc* deficiency had minor effect on the tumor growth in BALB/

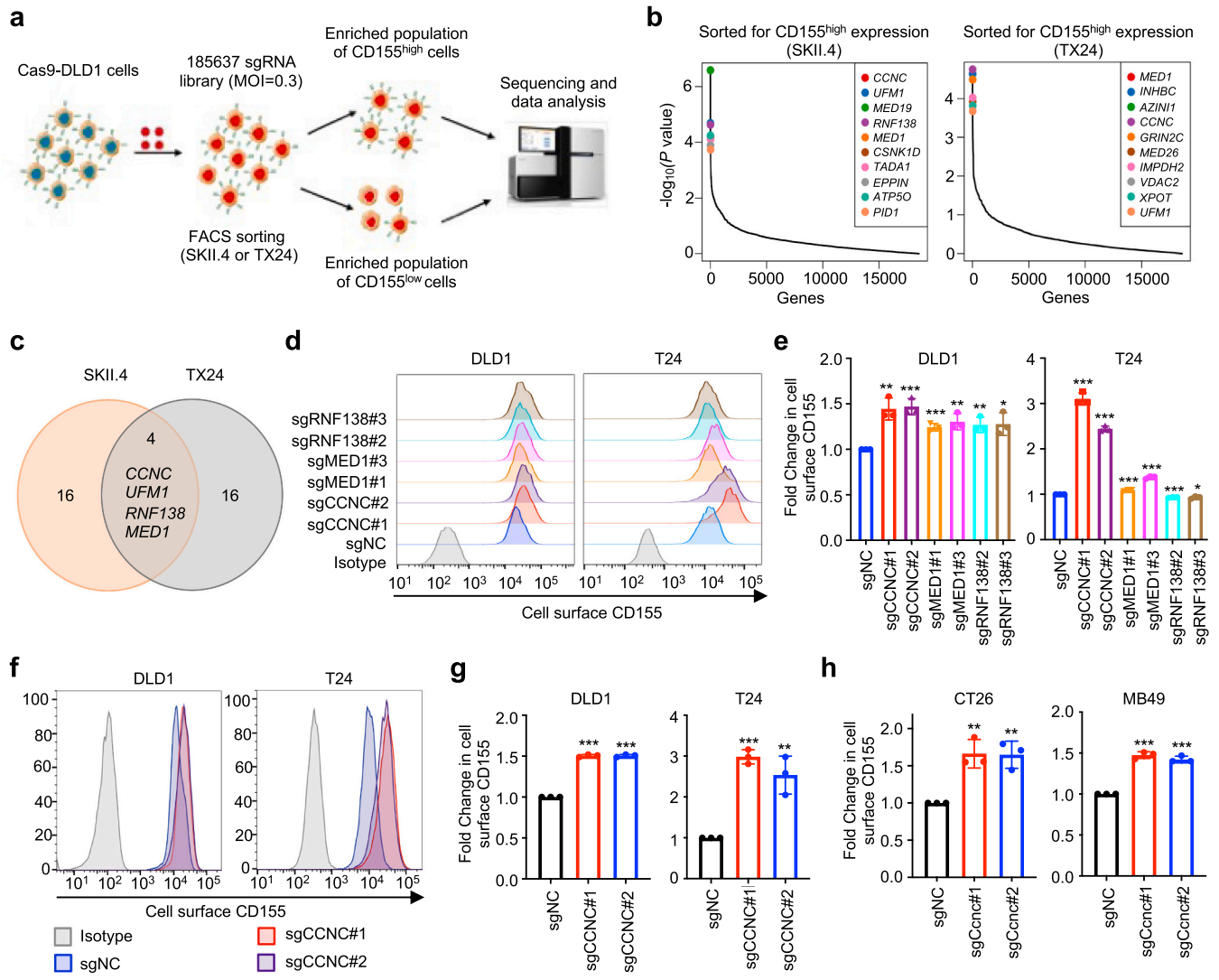

Fig. 1. Identification of CCNC as a modulator of CD155 expression. **a** A schema showing the procedures of the genome-wide CRISPR–Cas9 screening for regulators of CD155. **b** Top 10 regulators sorted for high CD155 expression with two human CD155 antibodies (clone SKII.4 and clone TX24). **c** Venn diagram of the Top 20 CD155 negative regulators. **d, e** Representative histograms (**d**) and quantification analysis (**e**) showing the surface levels of CD155 in human DLD1 and T24 cells with control and *CCNC*, *MED1*, and *RNF138* deficiency (n = 3). $^{*}P < 0.05$, $^{**}P < 0.01$, $^{***}P < 0.001$, by unpaired t test. **f, g** Representative histograms (**f**) and quantification analysis (**g**) showing the surface levels of CD155 in human DLD1 and T24 cells with control and *CCNC* deficiency (n = 3). $^{**}P < 0.01$, $^{***}P < 0.001$, by unpaired t test. **h** Bar plots showing the surface levels of CD155 in murine MB49 and CT26 cells with control and *Ccnc* deficiency (n = 3). $^{**}P < 0.01$, $^{***}P < 0.001$, by unpaired t test.

c-nude mice (Supplementary Fig. S2d), which possess functional NK and other innate immune cells but are deficient of T and B cells. We performed experiments with immunocompetent mice and found that *Ccnc* deficiency increased the tumor volume in wild-type C57BL/6 mice (Fig. 2a), suggesting *Ccnc* deficiency may promote immune evasion. CD155 is a ligand of TIGIT, which can transduce inhibitory signals to $CD8^+$ T and NK cells and suppress anti-tumor immunity (Tahara-Hanaoka et al., 2006). We examined tumor immune microenvironment and found that *Ccnc* deficient tumors had a lower frequency of tumor-infiltrating $CD8^+$ T and NK cells (Fig. 2b). These results indicate that CCNC remodels immune microenvironment and tumor immunity through T and NK cells.

As CD155 has been known to promote functional exhaustion of immune effector cells in tumor microenvironment, we evaluated the effects of *Ccnc* deficiency on T cell responses by co-culturing tumor cells with T cells. Our data showed that *Ccnc* deficient MB49 cells were killed less efficiently by primary activated mouse T cells (Fig. 2c). We also evaluated the effects of *CCNC* deficiency on NK92 cell responses and found that *CCNC* deficient T24 cells and DLD1 cells were killed less efficiently by NK92 cells (Fig. 2d, e, and Supplementary Fig. S2e). Importantly, knockout of *CD155* blocked the effect of *CCNC* deficiency on NK cell mediated killing function (Fig. 2f). These data suggest that *Ccnc* deficiency promotes functional exhaustion of immune effector cells and confers resistance to NK and T cell-mediated killing in a CD155-dependent manner.

Next, monoclonal antibody (mAb) against TIGIT significantly inhibited tumor growth in mice bearing control (sgNC) tumors, whereas this anti-tumor effect was markedly attenuated in mice bearing Ccnc-deficient tumors (Fig. 3a–c). These results indicate that loss of *Ccnc* increases resistance to TIGIT blockade and promotes immune evasion through upregulation of CD155 and suppressing the levels of infiltrating immune cells.

It has been known that the coordinated function of PD-1/PD-L1 and TIGIT/CD155 axes dampen anti-tumor immune responses, and co-blockade of PD-1/PD-L1 and TIGIT/CD155 demonstrated synergy in preclinical models and in early-stage clinical trials (Chu et al., 2023; Cho et al., 2022; Banta et al., 2022b). Interestingly, we found that PD-1 blockade reduced both the control and *Ccnc* deficient tumor growth

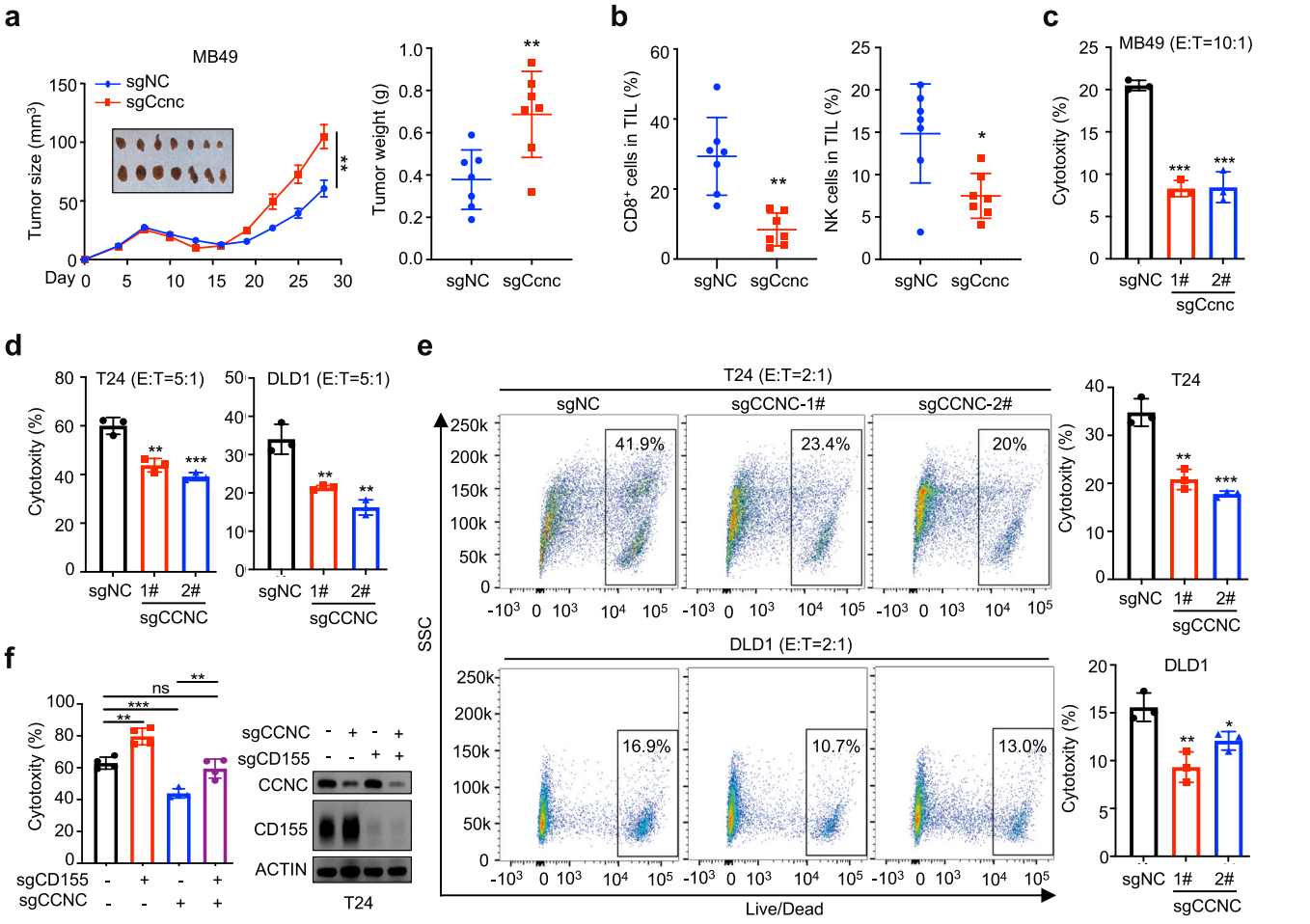

Fig. 2. *Ccnc* deficiency suppresses T and NK cells function through CD155/TIGIT. a The tumor images, tumor sizes and weights of the control and *Ccnc* deficiency tumors (n = 7). $^{**}P < 0.01$, by unpaired t test. **b** Quantification of tumor-infiltrating $CD8^+$ T and NK cells by flow cytometric analyses. $^{*}P < 0.05$, $^{***}P < 0.001$, by unpaired t test. **c** LDH release assay showing the cytotoxicity of control and *Ccnc* deficient MB49 cells killed by the primary activated T cells derived from mice (n = 3). $^{***}P < 0.001$, by unpaired t test. **d** LDH release assay showing the cytotoxicity of control and *CCNC* deficient T24 and DLD1 cells killed by NK92 cells (n = 3). $^{**}P < 0.01$, $^{***}P < 0.001$, by unpaired t test. **e** Flow cytometric and quantification analyses showing the percentages of control and *CCNC* deficient T24 cells and DLD1 cells killed by NK92 cells (n = 3). $^{**}P < 0.01$, $^{***}P < 0.001$, by unpaired t test. **f** LDH release assay showing the normalized cytotoxicity of control, *CCNC* deficient, CD155 deficient, and CCNC and CD155 double deficient T24 cells killed by NK92 cells (n = 6). $^{**}P < 0.01$, by unpaired t test. Western blot to validate the knockout efficiency of CCNC and CD155 in T24 cells.

(Fig. 3d-g). Additionally, anti-TIGIT and anti-PD-1 combined therapy was effective in *Ccnc* deficient tumors, indicating that dual blockade may overcome monotherapy resistance in these tumors (Fig. 3c-h). These data suggest that the combination of TIGIT and PD-1 blockade can overcome pre-existing or acquired resistance to immunotherapy in *Ccnc*-loss tumors, highlighting that tumors harboring *CCNC* loss may require combinatorial approaches to circumvent resistance to immunotherapy driven by CD155.

CCNC suppresses FOSL2-mediated CD155 transcriptional expression

We next explored the underlying mechanism by which CCNC up-regulates CD155. Given the essential significance of Mediator complex in a wide range of biological processes, as well as CCNC in gene transcription regulation, we examined the mRNA and protein level of CD155 in *CCNC* deficient tumor cells. It was found that CCNC suppresses CD155 transcriptional expression (Fig. 4a, b, and Supplementary Fig. S3a). To further identify how CCNC regulates CD155 expression, we performed RNA sequencing analysis and found that 180 genes were significantly up-regulated and 21 genes down-regulated in *CCNC* deficient tumor cells (Fig. 4c and Supplementary Fig. S3b). The Gene Ontology (GO) analysis showed that pathways related to virus infection, natural immunity, and intercellular signaling, including PVR, EB, Influenza A, Hepatitis C, NOD-like receptor signaling, cell adhesion molecules, and ECM-receptor interaction, are elevated in *CCNC* deficient cells (Fig. 4d).

Previous studies have shown that CCNC can regulate the transcriptional activity of multiple transcription factors (TFs) through the Mediator complex Cyclin-Dependent Kinase module (CKM) module (Fang et al., 2022). We therefore examined whether CCNC suppresses CD155 expression via regulating the transcriptional activity of any transcription factor. To this end, we inferred the potential TFs underlying the significant differentially expressed genes(DEGs) (Fig. 4c) using LISA model, which has been demonstrated as an efficient software to predict the potential TFs. We found that AP-1, TEAD, and CEBP families of transcription factors are the potential TFs regulated by CCNC (Supplementary Fig. S3c; Supplementary Table S2). The top 20 transcription factors predicted by LISA from our RNA-seq data and GSE150067 data (Tang et al., 2021) were intersected to obtain FOSL2, FOS, ATF3 and JUN of AP-1 family (Fig. 4e and Supplementary Fig. S3c). Further analysis from TCGA database revealed a positive correlation between FOSL2 and CD155 expression across 30 cancer types (Supplementary Fig. S3d), suggesting that FOSL2 could be a potential transcription factor involved in the CCNC mediated CD155 expression.

We examined whether CD155 expression is regulated by FOSL2. Our

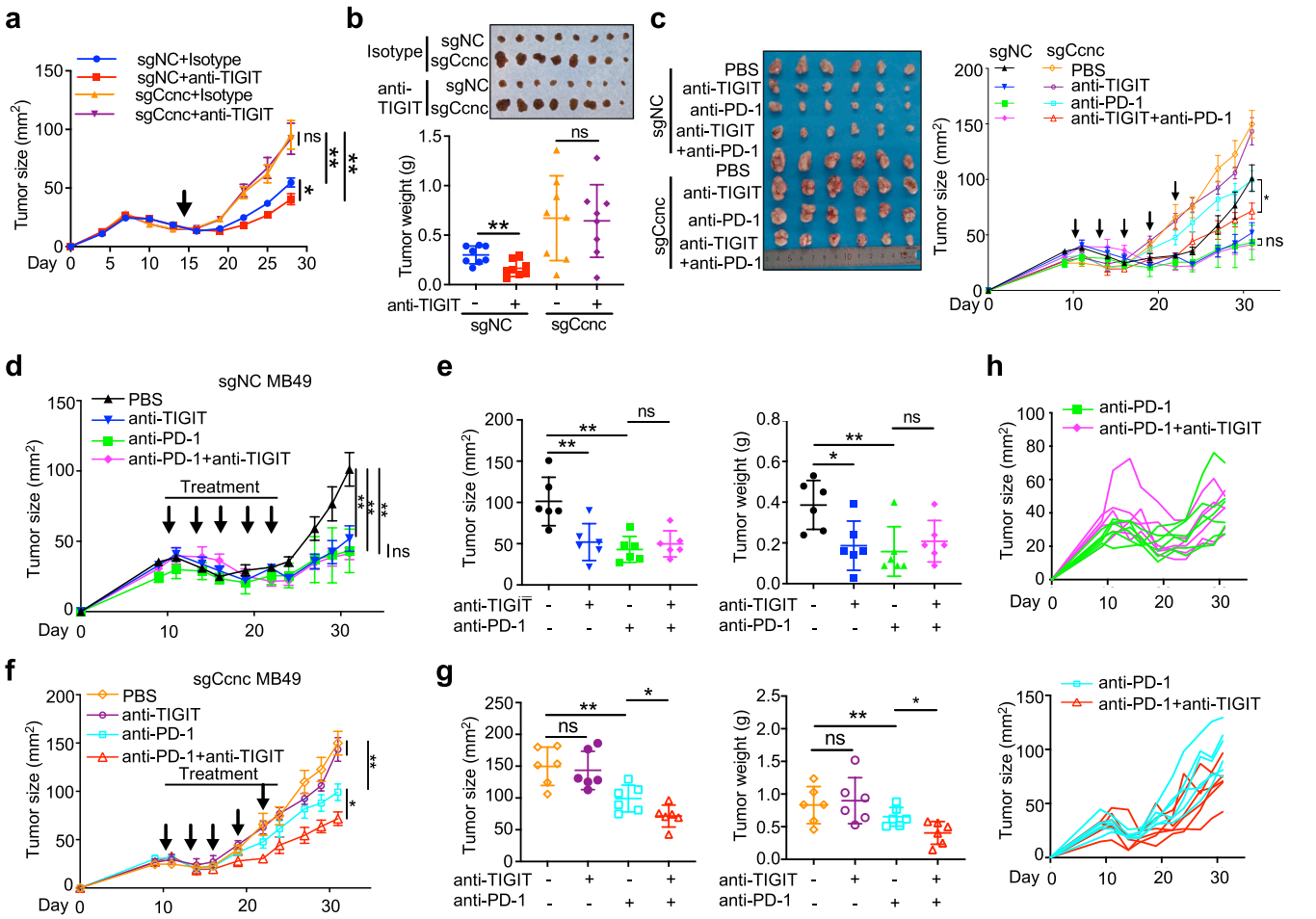

Fig. 3. ***Ccnc*** **deficiency confers resistance to anti-TIGIT therapy and sensitizes tumors to TIGIT/PD-1 combination blockade. a, b** The growth curve (**a**), representative image, and weights (**b**) of the control and *Ccnc* deficient MB49 tumors in C57BL/6 mouse treated with anti-TIGIT antibodies (n = 8). $^{**}P < 0.01$, by unpaired t test. c The growth curve and representative image of the control and *Ccnc* deficient MB49 tumors in C57BL/6 mouse treated with mono-ICB (PD-1, TIGIT) or dual-ICB (PD-1/TIGIT) antibodies. $^{*}P < 0.05$, by unpaired t test. d The growth curve of the control MB49 tumors in C57BL/6 mouse treated with mono-ICB (PD-1, TIGIT) or dual-ICB (PD-1/TIGIT) antibodies. $^{**}P < 0.01$, by unpaired t test. e The tumor size and weights of the control MB49 tumors at day 31 (n = 6), $^{**}P < 0.01$, by unpaired t test. f The growth curve of the *Ccnc* deficient tumors in C57BL/6 mouse treated with mono-ICB (PD-1, TIGIT) or dual-ICB (PD-1/TIGIT) antibodies. $^{**}P < 0.01$, by unpaired t test. g The tumor size and weights of the *Ccnc* deficient tumors at day 31 (n = 6), $^{**}P < 0.01$, by unpaired t test. h The growth curve of control and *Ccnc* deficient tumors in each mouse.

data showed that *FOSL2* deficiency led to a decrease of CD155 mRNA and protein level (Fig. 4f). The decrease of CD155 in *FOSL2* deficient cells was further confirmed by flow cytometry (Fig. 4g). To determine whether FOSL2 can directly regulate the CD155 expression, we analyzed the potential binding elements of FOSL2 in the promoter of CD155 using JASPAR and identified three putative binding sites of FOSL2 in the promoter and enhancer of CD155 (Fig. 4h and Supplementary Fig. S3e). We performed ChIP-qPCR analysis and found that FOSL2 efficiently binds to the promoter and enhancer of CD155 (Fig. 4i). These data indicate that FOSL2 is a transcriptional factor of CD155 by directly binding to its promoter, thereby facilitating resistance to immunotherapy in CCNC-deficient tumor cells. Furthermore, we found that knockdown of *CCNC* abolished the effect of *FOSL2* deficiency on CD155 mRNA (Fig. 4j) and protein level (Fig. 4k). Additionally, *FOSL2* deficiency blocked the effect of *CCNC* knockdown on NK cell mediated killing function (Fig. 4l). Taken together, these results indicate that CCNC suppress the CD155 expression via FOSL2.

FBXO11 increases CCNC ubiquitination for degradation

We demonstrated that CCNC functions as a tumor suppressor by suppressing CD155 expression. We next explored the underlying mechanism by which CCNC is suppressed in cancer cells. It was found that cycloheximide (CHX), a small-molecule inhibitor of new protein synthesis, decreased CCNC protein levels in a time-dependent manner. Additionally, MG132 (Carbobenzoxy-L-leucyl-L-leucyl-L-leucinal), a proteasome inhibitor, and MLN4924 (Pevonedistat), a small-molecule inhibitor of the Neural precursorcell-expressed developmentally down-regulated 8 (NEDD8)-activating enzyme (NAE) that inactivates cullin-RING ligases (CRLs) by inhibiting Cullin neddylation, significantly stabilized CCNC (Fig. 5a), suggesting that the protein stability of CCNC can be regulated by Cullin-dependent E3 ubiquitin ligases.

To further identify the candidate E3 ligase(s) that may target CCNC for degradation, we re-analyzed our CRISPR screen data in the $CD155^{low}$ populations that may positively regulate CD155 expression. sgRNAs corresponding to sites within 1426 and 875 genes were significantly enriched in SKII.4 and TX24 antibody group, respectively (Supplementary Table S3). Except CD155 (PVR), the most significantly enriched one of these genes were single guide RNAs targeting *FBXO11*, a Cullin-dependent E3 ligase, was identified to regulate CD155 expression (Fig. 5b, and Supplementary Fig. S4a, b). Additionally, FBXO11 was also predicted as the potential E3 ligase of CCNC identified by UbiBrowerse online tool (Fig. 5c). To further confirm whether FBXO11 is an E3 for CCNC, we generated human and mouse *FBXO11* deficient cancer cells

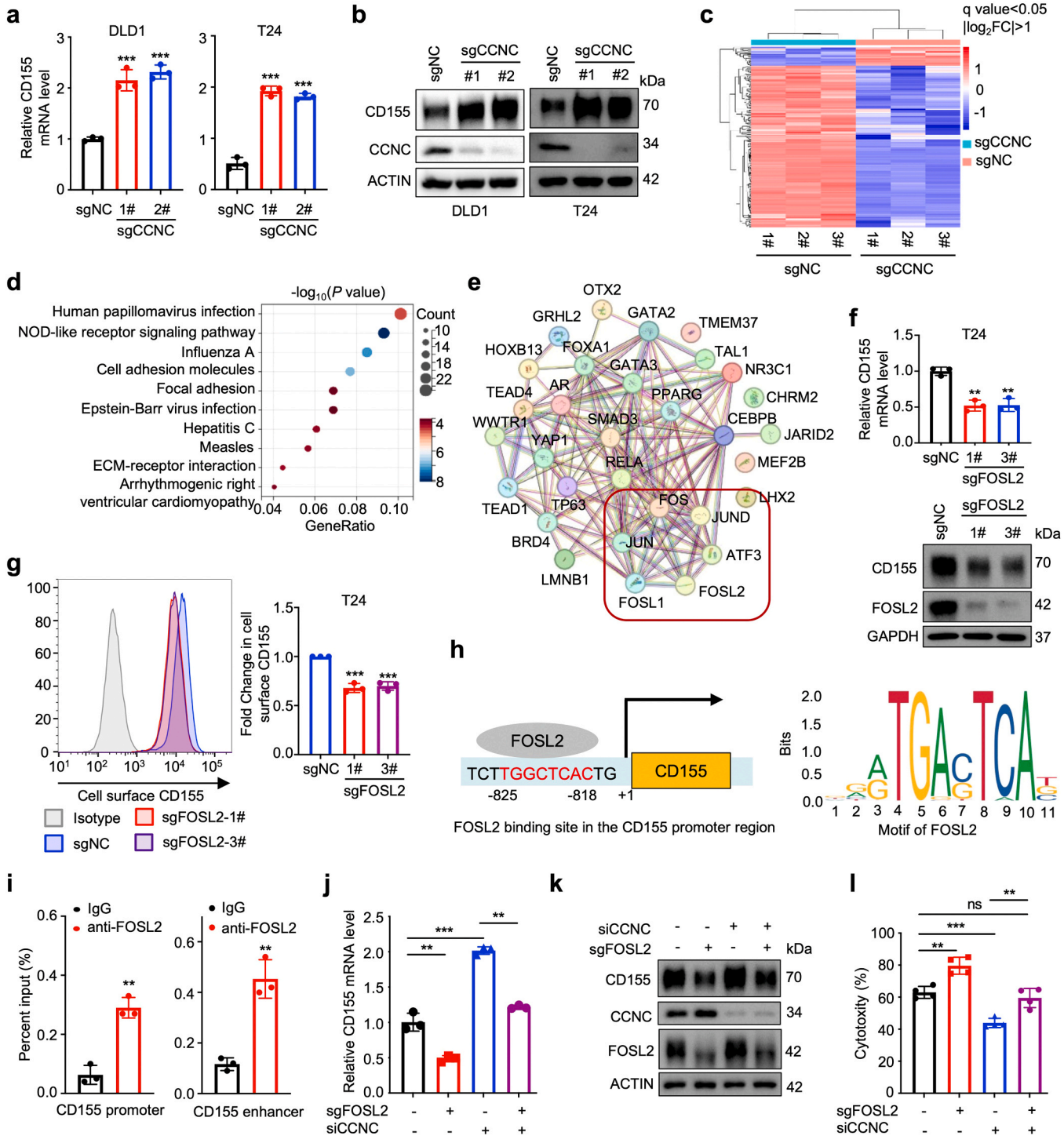

Fig. 4. CCNC suppresses FOSL2-mediated CD155 transcriptional expression. a Real-time qPCR validating CD155 expression in control and *CCNC* deficient DLD1 and T24 cells. ***$P < 0.001$, by unpaired t test. **b** Western **b**lot showing the protein level of CD155 in control and *CCNC* deficient DLD1 and T24 cells. **c** Heatmap showing differential transcriptomic expression in control and *CCNC* deficient T24 cells. **d** Gene set enrichment analysis of upregulated genes in *CCNC* deficient compared to control T24 cells. Top enrichment pathways are shown. **e** LISA predicts transcription factors in upregulated genes. **f** Relative mRNA and protein levels of CD155 in control and *FOSL2* deficient T24 cells. Data are shown as mean ± SD, 3 replicates per condition. **$P < 0.01$, by unpaired t test. **g** Flow cytometry (left) and quantification (right) analyses showing membrane CD155 expression in control and *FOSL2* deficient T24 cells. ***$P < 0.001$, by unpaired t test. **h** Schematic diagram of FOSL2 binding site (left) and FOSL2 binding motif (right) on CD155 promoter. **i** ChIP assay to validate FOSL2 **b**inding to CD155 promoter and enhancer in T24 cells, **$P < 0.01$, by unpaired t test. **j** Real-time qPCR to validate CD155 expression in sgNC+siNC, sgFOSL2 +siNC, sgNC+siCCNC, and sgFOSL2 + siCCNC cancer cells. Data are shown as mean ± SD, 3 replicates per condition, **$P < 0.01$, ***$P < 0.001$, by unpaired t test. **k** Western blot showing the protein level of CD155, CCNC, and FOSL2 in sgNC+siNC, sgFOSL2 +siNC, sgNC+siCCNC, and sgFOSL2 + siCCNC T24 cells. **l** LDH release assay to validate the cytotoxicity of sgNC+siNC, sgFOSL2 +siNC, sgNC+siCCNC, and sgFOSL2 + siCCNC T24 cells killed by NK92 cells. n = 4. **$P < 0.01$, ***$P < 0.001$, by unpaired t test.

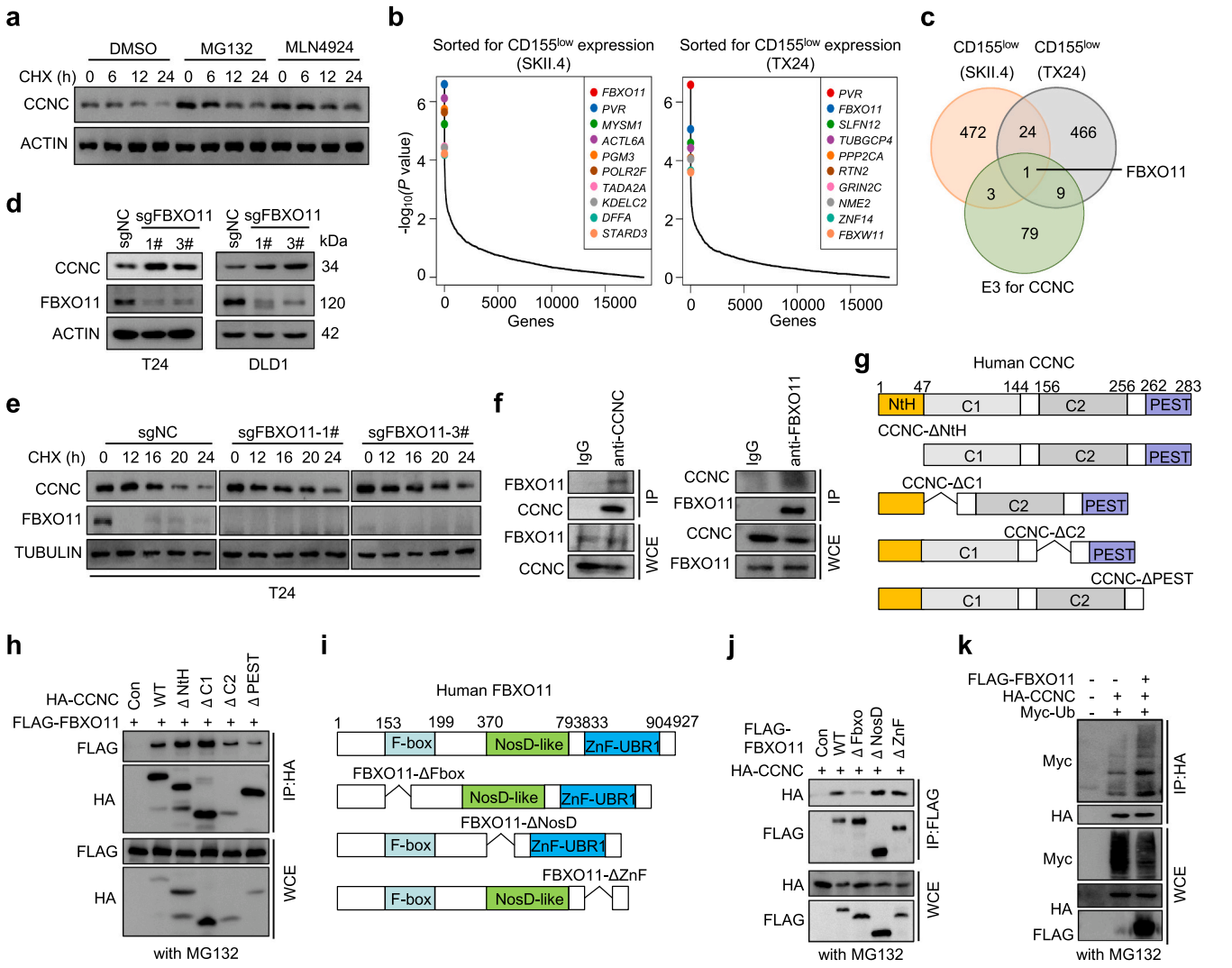

Fig. 5. FBXO11 increases CCNC ubiquitination for degradation. **a** T24 cells treated with MG132 (10 μM) or MLN4924 (10 μM) for 5 hr before cycloheximide (CHX,10 μg/ml) treatment as indicated. Protein levels of CCNC were analyzed by Western blotting. **b** Top 10 regulators sorted for low CD155 expression with two human CD155 antibodies (clone SKII.4 and clone TX24). **c** Venn diagram of predicted E3 ubiquitin ligase for CCNC by UbiBrowser 1.0 and the top 500 positive CD155 regulators in genome-wide CRISPR–Cas9 screening. **d** Western blot showing the protein levels of CCNC and FBXO11 in sgFBXO11 and sgNC T24 and DLD1 cells. **e** Western blot showing the protein levels of CCNC and FBXO11 in sgFBXO11 and sgNC T24 cells treating cells with cycloheximide (CHX,10 μg/ml) as indicated. **f** Endogenous interaction between CCNC and FBXO11 was detected in sgNC, sgCCNC, and sgFBXO11 T24 cells. **g** Schematic representation of CCNC domain and deletion mutants. **h** FLAG-FBXO11 and HA-CCNC WT or deletion mutants were co-expressed in HEK293T cells. After treatment with MG132 (10 mM) for 5 hr, the Co-IP assay was performed and analyzed by Western blot. **i** Schematic representation of FBXO11 domain and deletion mutants. **j** HA-CCNC and FLAG-FBXO11-WT or deletion mutants were co-expressed in HEK293T cells. After treatment with MG132 (10 mM) for 5 hr, the Co-IP assay was performed and analyzed by Western blot. **k** HA-CCNC, FLAG-FBXO11, and Myc-ubiquitin were co-expressed in HEK293T cells. After treatment with MG132 (10 mM) for 5 hr, the nickel-nitrilotriacetic acid (Ni-NTA) ubiquitination assay was performed and analyzed by Western blot.

and found that *FBXO11* deficiency increased CCNC expression (Fig. 5d) and extended the protein half-life of endogenous CCNC (Fig. 5e and Supplementary Fig. S4c), but had no effect on CCNC transcription (Supplementary Fig. S4d). Thus, FBXO11 is proposed to be an E3 for CCNC.

Next, FBXO11 binding to CCNC was confirmed with endogenous and exogeneous expressed FBXO11 and CCNC (Fig. 5f and Supplementary Fig. S4e). Additionally, the F-box domain of FBXO11 and the PEST domain of CCNC were required for their interaction (Fig. 5g-j). Importantly, FBXO11 increased the polyubiquitination of CCNC (Fig. 5k). Deletion of the F-box domain partially impaired FBXO11-increased the polyubiquitination of CCNC (Supplementary Fig. S4f). Taken together, these results indicate that FBXO11 is an E3 ligase for CCNC to promote its ubiquitination and degradation.

FBXO11 deficiency suppresses CD155 expression dependent on CCNC

We next examined whether FBXO11 regulates CD155 expression. We found that *FBXO11* deficiency suppressed the protein (Fig. 6a) and mRNA (Fig. 6b) level of CD155. Additionally, *CCNC* deficiency abolished the effect of *FBXO11* deficiency on CD155 protein (Fig. 6c) and mRNA level (Fig. 6d), suggesting FBXO11 suppressed CD155 transcription in a CCNC dependent manner. Furthermore, we also found that *FBXO11* deficiency suppressed cell surface CD155 (Fig. 6e) via CCNC (Fig. 6f). Consistently, *FBXO11* deficient tumor cells were killed more efficiently by NK92 cells (Fig. 6g), while *CCNC* deficiency blocked the effect of *FBXO11* deficiency on NK cell mediated killing function (Fig. 6h). Collectively, these data suggest that FBXO11 suppressed the protein stability of CCNC to inhibit CD155 transcription, which suppressed NK cell mediated killing function and promoted tumor

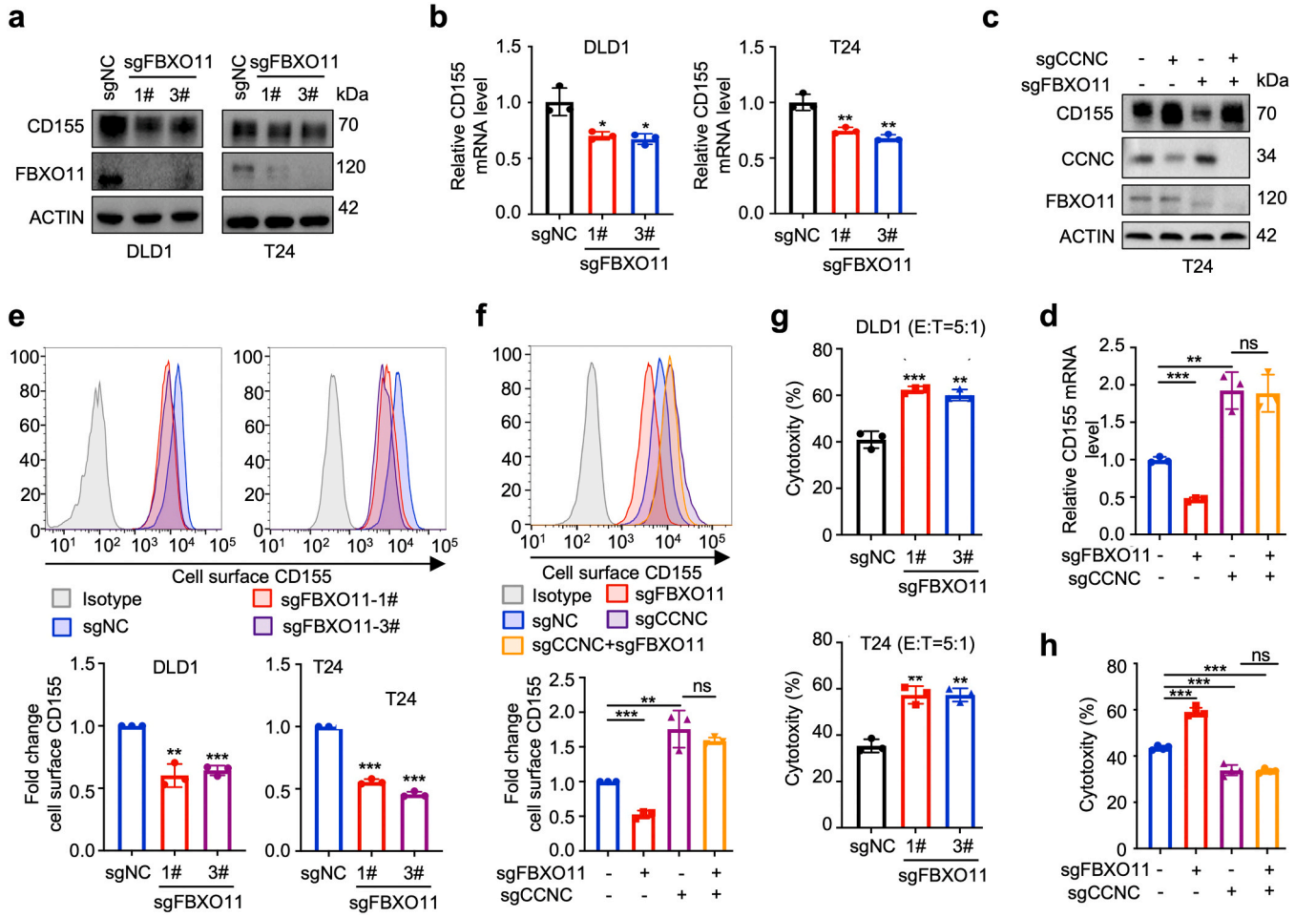

Fig. 6. ***FBXO11*** **deficiency suppresses CD155 expression dependent on CCNC. a** Western blot validating CD155 expression in *FBXO11* knockout DLD1 and T24 cells. **b** Real-time qPCR validating CD155 expression in *FBXO11* knockout in DLD1 and T24 cells, $^{*}P < 0.05$, $^{**}P < 0.01$, by unpaired t test. **c, d** Western blot (**c**) and Real-time qPCR (**d**) validating the expression of CD155, CCNC, and FBXO11 in sgNC, sgCCNC, sgFBXO11, and sgCCNC+sgFBXO11 T24 cells. **e** Flow cytometry (above**e**) and quantification (below) analyses showing the surface level of CD155 in control and *FBXO11* deficient DLD1 and T24 cells (n = 3). **f** Flow cytometry (above) and quantification (below) analyses showing membrane CD155 expression in sgNC, sgCCNC, sgFBXO11, and sgCCNC+sgFBXO11 T24 cells (n = 3). **g** LDH release assay to validate the cytotoxicity of control and *FBXO11* deficient T24 (below) or DLD1 (above) cells killed by NK92 cells (n = 3). **h**, LDH release assay to validate the cytotoxity of sgNC, sgCCNC, sgFBXO11, and sgCCNC+sgFBXO11 T24 cells killed by the NK92 cells (n = 3). Data are shown as mean ± SD, 3 replicates per condition, $^{**}P < 0.01$, $^{***}P < 0.001$, by unpaired t test.

resistance to immune effector activity.

CCNC expression is negatively correlated with CD155 expression in cancers

To investigate the correlation between the expression of CCNC and CD155 in clinical tumors, immunofluorescence staining was performed on tissue microarray samples containing 48 cases of urothelial carcinoma. Our data showed that the level of CCNC protein was reversely correlated with CD155 expression (Figs. 7a and 7b). In addition, the mRNA expression of CCNC were negatively correlated with CD155 in TCGA cohorts with colon adenocarcinoma (COAD) and kidney clear cell carcinoma (KIRC) (Fig. 7c). TCGA data analysis also showed that CCNC was downregulated in KIRC, and Skin Cutaneous Melanoma (SKCM) tumor tissues (Supplementary Fig. S5a). Furthermore, high CCNC expression was related to good prognosis (Supplementary Fig. S5b) and infiltration of NK and $CD8^{+}$ T cells (Supplementary Fig. S5c) in KIRC and SKCM tumors. Consistently, our urothelial carcinoma cohort also confirmed that high CCNC expression predicted better prognosis (Fig. 7d). Additionally, high CCNC expression was related to good prognosis with PD-1/PD-L1 blockade therapy in pan-cancers (Fig. 7e and Supplementary Fig. S5d). These data suggest that CCNC expression is negatively correlated with CD155 expression and functions as a tumor suppressor for good clinical outcome.

Reversely, FBXO11 was highly expressed in multiple cancers by TNMplot (Supplementary Fig. S5e). High expression of FBXO11 was positively correlated to CD155 (Supplementary Fig. S5f) and negatively correlated with infiltration of NK and $CD8^{+}$ T cells (Supplementary Fig. S5g). Additionally, high expression of FBXO11 had a poor prognosis in cancer patients treated with PD-L1 blockade therapy (Supplementary Fig. S5h), suggesting that FBXO11 positively regulates CD155 and promotes cancer immune evasion.

Discussion

Immunotherapy is emerged as a new type of clinical treatment for cancer. CD155 is an important inhibitory immune checkpoint on the surface of tumor cells, which mediates immune evasion and participate in tumor malignant progression (Freed-Pastor et al., 2021; Briukhovetska et al., 2023; Braun et al., 2020b). CD155 on cancer cells leads to functional exhaustion of T and NK cells and induces immune escape by binding to inhibitory receptors TIGIT, CD96, or costimulatory receptor CD226 (O'Donnell et al., 2020). Clinical data support that targeted TIGIT therapy has achieved durable clinical benefit (Lepletier et al.,

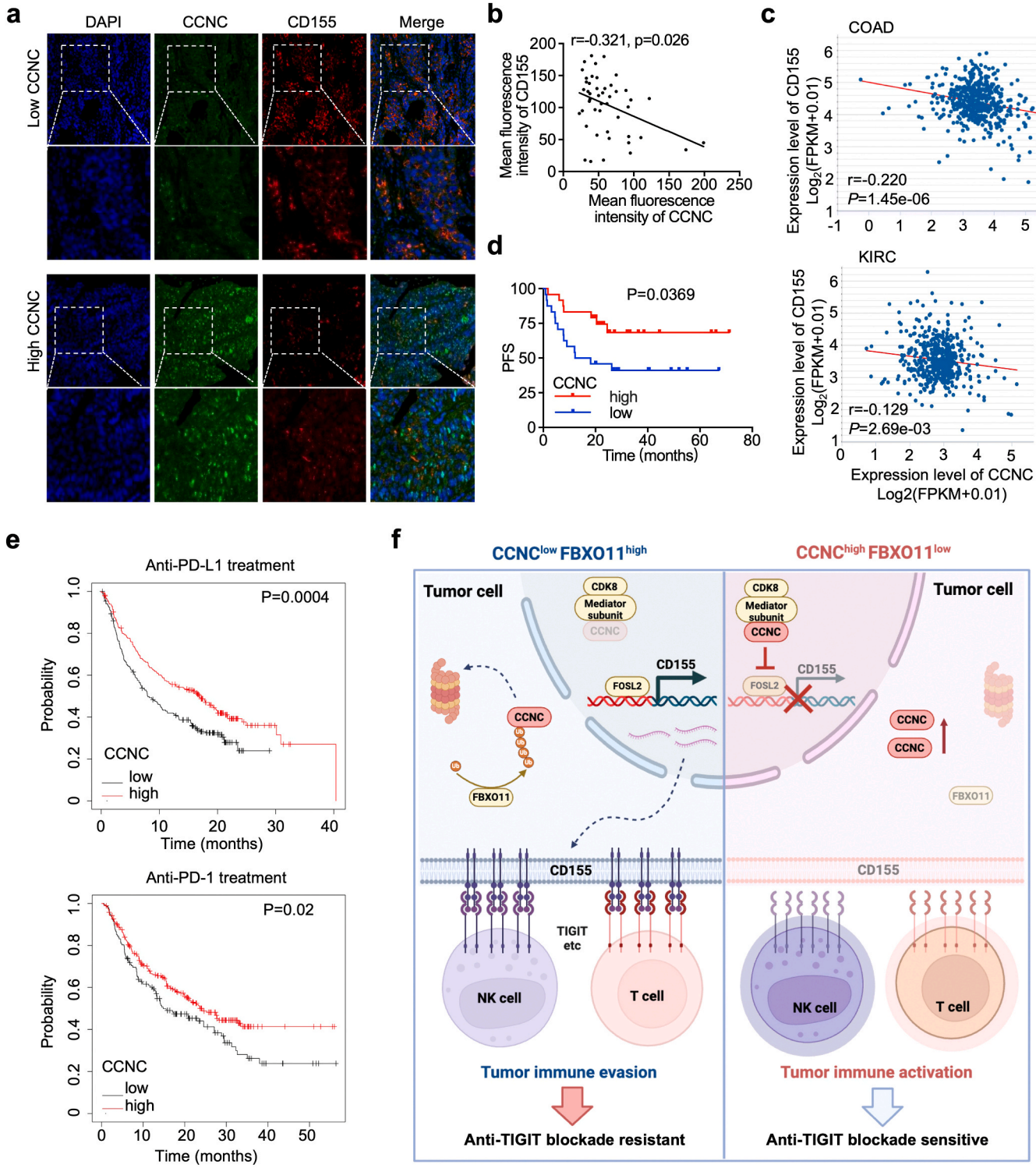

Fig. 7. CCNC expression is negatively correlated with CD155 in cancers. a Representative image of CCNC and CD155 expression in urothelial carcinoma from patients. Scale bar,10 × (up), 20 × (down). **b** Correlation between CCNC and CD155 in 48 urothelial carcinoma samples. The protein abundance was quantified by ImageJ and plotted by Graphpad Prism 9. **c** Correlation between CD155 and CCNC in COAD and KIRC from TCGA database. **d** Kaplan-Meier analysis of progression-free survival (PFS) in a set of 48 urothelial cancer patients with CCNC expression. Log-rank test, $p = 0.0369$. **e** Overall survival based on CCNC expression in pan-cancer patients treated with immune-checkpoint inhibitors and analyzed by KM-plotter, including anti-PD-L1 and anti-PD-1 treatment. **f** A model of CCNC functions as a suppressor of CD155-mediated cancer immune evasion.

2020). Therefore, a deeper understanding on the regulation of CD155 is essential for optimizing immunotherapy interventions.

To broaden knowledge about the factors that drive the high expression of CD155, we performed the whole-genome CRISPR-Cas9 screens. Dozens of genes participate in CD155 biogenesis and turnover. These genes function in diverse cellular pathways ranging from epigenetic control to protein trafficking and markedly enriched in Mediator complex (Chen et al., 2021a). In this study, we found that loss of *CCNC*

led to the up-regulation of CD155 at transcriptional level. Functionally, *CCNC* deletion reduces the antitumor activity of NK and T cells in a CD155-dependent manner *in vitro*. Mechanically, we found that loss of *CCNC* up-regulates CD155 via the transcription factor FOSL2. Additionally, we found that FBXO11 up-regulates the expression of CD155 by promoting the ubiquitination and degradation of CCNC. We also observed the correlation between CCNC expression and NK cell infiltration in human cancers. Taken together, this study establishes the molecular mechanism by which FBXO11 regulates CCNC stability through ubiquitination, and CCNC transcriptionally regulates CD155 expression through transcriptional factor FOSL2, shaping the immune microenvironment and dictating tumor resistance to immune checkpoint blockade. *In vivo* experiments confirmed the function of CCNC in tumor immune escape, and uncovered that CCNC was required for anti-TIGIT blockade and low CCNC expression could be an indication for the combined application of anti-TIGIT and anti-PD-L1 antibodies for immunotherapy (Fig. 7f).

Previous studies have demonstrated that dysregulation of CCNC plays important roles in tumorigenesis. CCNC deletion can increase the stability of Notch1 intracellular domain ICN1 and promote the malignant progression of acute T-lymphocyte leukemia (Li et al., 2014). In addition, CCNC deletion was found to be closely related to the drug resistance of ATR inhibitors and PARP inhibitors (Tang et al., 2021; Lloyd et al., 2021). However, other studies also reveal that the CCNC gene is amplified and significantly associated with poor prognosis in breast cancer (Broude et al., 2015). In the present study, we found the effect of CCNC on NK and T cell responses and immune evasion through CD155 in solid tumors, suggesting that CCNC is essential for blocking the effect of immune escape by TIGIT antibody to inhibit tumor growth. These findings imply that CCNC loss may serve as a molecular driver of resistance to immune checkpoint therapies targeting the TIGIT/CD155 axis.

In human, the Mediator complex consists of 30 protein subunits, including Mediator core module and CDK8 kinase module (Rengachari et al., 2021). CKM module reversibly combines with Mediator core module to regulate the transcription process (Chen et al., 2021a). Studies have shown that CCNC can regulate the transcriptional activity of multiple TFs through the Mediator complex CKM module, including TFIIH, p53, E2F1, Notch intracellular domain and Smad (Xu and Ji, 2011). LISA analysis of the genes upregulated upon CCNC KO implicated the AP-1, TEAD, and CEBP families of transcription factors as putative regulators. Using the LISA model based on ChIP-seq motifs of genes upregulated upon CCNC knockout, we identified FOSL2 as one of the most significantly altered members of the AP-1 transcription factor family. This suggests that FOSL2 may be involved in CD155-mediated resistance to immune effector cells. We found that FOSL2 can bind to the promoter and enhancer regions of CD155, thus having the ability to directly regulate its expression. Furthermore, knockout of *FOSL2* down-regulated CD155 expression. Importantly, deletion of *FOSL2* abolished CD155 gene expression induced by the *CCNC* deficiency. FOSL2 contributes to CD155-mediated immune escape caused by *CCNC* deletion. Fibroblast growth factor (FGF) has been reported to upregulate CD155 expression through Raf-MEK-ERK-AP1 signaling (Hirota et al., 2005). FOSL2 is a component of the dimeric transcription factor activator protein-1 (AP-1), which is composed of FOS, JUN, activating transcription factor (ATF), and MAF protein families (Chen et al., 2021b). Moreover, studies have found that FOSL2 is highly expressed in a variety of tumors, promotes the proliferation, migration, and invasion of tumor cells, suggesting that FOSL2 associated with the occurrence and development of tumors (Bejjani et al., 2021; Bian et al., 2021; Higuchi et al., 2013). In contrast, another study reported that FOSL2 is downregulated in melanoma where downregulation of FOSL2 promotes the metastatic potential of melanoma cells by upregulation of Fam212b (Chen et al., 2021b). We note that FOSL2 is not the only AP-1 family member whose transcriptional activity are affected. It is possible that loss of *CCNC* could enhance transcriptional activity of other AP-1 family members which function in promoting CD155 expression and immune evasion. In addition, our RNA-seq analysis suggest that the TEAD family of transcription factors might activate the transcriptional expression of CD155 upon *CCNC* deficiency. In agreement with this, a previous study indicated that CD155 is the direct target of YAP and is driven by YAP phase separation, which partitions with TAZ, TEAD4, EP300, and MED1 to form condensates (Yu et al., 2021). Collectively, these results suggest that CCNC plays a major role in CD155 expression by serving as a pivotal modulator to integrate the effects of FOSL2 transcriptional activity.

Despite its relevance to immunotherapy resistance, there are few reports on the ubiquitination regulation of CCNC. A recent study shows that E3 ubiquitin ligase HACE1 can mediate ubiquitination modification of CCNC without affecting CCNC degradation, thereby promoting its nuclear-mitochondrial translocation and chemotherapy resistance in gastric cancer cells (Fang et al., 2022). However, how CCNC is ubiquitinated and degraded by E3 ligase, remains largely unknow. We identified that FBXO11 is the E3 ubiquitin ligase of CCNC, and FBXO11 is an important member of F-bxo subfamily, which controls cell cycle, tumor development and metastasis. Additionally, we proved that FBXO11 regulates the expression of CD155 through ubiquitination and degradation of CCNC.

Recent studies have shown the important role of FBXO11 in tumor immunity. It is reported that FBXO11 promotes CD40 expression by targeting repressors CTBP1 and BCL6 (Jiang et al., 2019). Moreover, FBXO11 can mediate the degradation of CIITA, which is the main transcription factor regulating MHC class II expression, thereby exerting a strong anti-tumor immune response (Chan et al., 2022). Although ABC transporters such as P-glycoprotein (ABCB1) and breast cancer resistance protein (ABCG2) are well-known contributors to chemotherapy resistance by actively exporting cytotoxic drugs out of tumor cells (Gose et al., 2024; Zhang et al., 2024), our genome-wide CRISPR-Cas9 screen did not identify these transporters as regulators of CD155-mediated immune evasion. This finding suggests that classic multidrug resistance mechanisms mediated by ABC transporters may not be directly involved in resistance to immune checkpoint blockade, such as anti-TIGIT or anti-PD-1 therapy. Instead, our data highlight that transcriptional and post-translational regulation of CD155, particularly through the CCNC-FOSL2 axis and FBXO11-mediated degradation of CCNC, plays a more prominent role in shaping resistance to immunotherapy. Targeting the FBXO11-CCNC axis represents a potential strategy for reversing CD155 mediated immune resistance. It should be feasible to develop new drugs by linking E3 ligase inhibitors (such as Pevonidistat/MLN4924) with PROTAC in the future. Therefore, targeting immune-specific regulatory pathways, rather than general drug efflux mechanisms, may offer more effective strategies for overcoming resistance to immunotherapy.

This study has several limitations. (1) this study focused on the MB49 bladder cancer model in which sex-specific was not considered. Although the observed male-female variation in anti-tumor immunity has not been fully explained, sex-biased differences have been evident in epigenetic regulation of gene expression, cellular senescence, microbiota composition, metabolism, and DNA damage response, all of which impact anti-tumor immunity and immunotherapy treatment efficacy (Yang et al., 2022; Hargrove-Wiley and Fingleton, 2023; Alspach, 2023; Tao et al., 2025). Thus, future validation in both sexes is important. (2) We have demonstrated that low CCNC expression or high FBXO11 expression is significantly associated with high CD155 expression, poor tumor prognosis, and inferior immunotherapy outcomes across various cancer types. However, the reliability of the combination of low CCNC expression and high FBXO11 expression as a predictive biomarker for immunotherapy response requires further exploration.

In summary, our findings identified CCNC as a novel modulator of CD155 expression, loss of which enhances CD155-mediated NK-cell suppression to induce immune evasion and resistance to immunotherapy. This study underscores the potential of CCNC as a predictive biomarker for immunotherapy resistance, particularly to anti-TIGIT

monotherapy.

Materials and methods

Cell lines

Human cells (including HEK293T cells, DLD1 colorectal cancer cells, T24 bladder cancer cells and NK leukemia cells) and mouse tumor cells (including MB49 bladder cancer cells and CT26 colorectal cancer cells) were obtained from ATCC. 293 T, DLD1, T24, MB49 and CT26 cells were cultured in DMEM (GIBCO) containing 10 % FBS (GIBCO) and 50 μg/ml penicillin/streptomycin (Invitrogeni) in a humid incubator with 5 % CO2 at 37°C. NK cells were cultured in NK-92 cell-specific medium (cat#: CM-0530) supplemented with IL-2 (PB180634). The RRIDs of cell lines were listed in Supplementary Table S4.

Mice

This study exclusively examined male mice. It is unknown whether the findings are relevant to female mice. For *in vivo* study, wild-type C57BL/6 mice and BALB/c nude male mice aged 6–8 weeks were obtained from Shanghai BIKAI Laboratory (China). All mouse procedures were conducted in compliance with the approved guidelines for animal experiments by the Animal Protection and Use Committee of Shanghai Tenth People's Hospital of Tongji University. The RRIDs of mice were listed in Supplementary Table S4.

Patient samples

This study was approved by the Institutional Review Committee of the Shanghai Tenth People's Hospital of Tongji University. All samples were collected with informed consent of patients. Tissue microarrays of human bladder cancer samples were provided by Shanghai Tenth People's Hospital, China. The diagnosis of human cancer tissue is confirmed based on the pathological findings of independent pathologists.

Plasmids

The cDNA of human FBXO11 wild-type, FBXO11-ΔFbox, FBXO11-ΔNOD and FBXO11-ΔZnF were cloned into pcDNA3.1-Flag expression vector. The cDNA of human CCNC wild-type, CCNC-ΔN, CCNC-ΔC1, CCNC-ΔC2, CCNC-ΔPEST were cloned into pLVX-puro-HA expression vector. Wild-type human ubiquitin (UBB) cDNA was cloned into pcDNA3.1-MYC expression vector. The sgRNA oligos were cloned into lenti-Guide-sgRNA-puro vector. The RRIDs of plasmids were listed in Supplementary Table S4.

CRISPR screening and DNA extraction

CRISPR screening was conducted following the previously described method (Chen and Mellman, 2017). A total of 2×10^8 DLD1 cells were infected with a human mixed lentivirus genome-wide sgRNA library (XBH) at a multiplicity of infection of 0.3 and selected with puromycin at a concentration of 1 μg/ml. After 7 days of appropriate selection, the cells were prepared for screening. The cells were collected by trypsinization and washed with PBS. They were then stained with PE anti-human CD155 antibody (Cat#337508, clone number: TX24; Cat#100553, clone number: SKII.4; Biolegend) for 30 min on ice and washed with PBS before undergoing sorting. Approximately 2 % of the cells expressing high and low levels of CD155 ($CD155^{high}$ and $CD155^{low}$, respectively) were enriched using FACS sorting.

Genomic DNA was extracted from both the sorted cells and the pooled cells using the previously described method (Kubli et al., 2021). The sgRNA sequences were amplified by PCR, and next-generation sequencing was performed by GENEWIZ. The analysis of the NGS data was carried out using XBH. MAGeCK-VISPR was utilized to perform the entire process, which includes data quality control, reading the atlas, sgRNA annotation, and condition comparison using the MAGeCK RRA algorithm. The positive selection genes and negative selection genes were selected based on the top 500 ranked by both FDR and a cut off P-value of 0.05. For each genome, GO term enrichment and KEGG pathway enrichment analyses were conducted using DAVID.

Generation of CRISPR-Cas9 knockout cell lines

For *FBXO11*, *CCNC*, *FOSL2*, or *MED1* knockout cell lines, sgRNAs targeting each gene were cloned into the lentiCRISPR-V2 vector for lentivirus production. DLD1, T24, MB49, and CT26 cells were infected with lentivirus Cas9 for 24 h, and Cas9-integrated cells were selected using 10 μg/ml blasticidin (60218ES60, Yeasen Biotechnology) until all lentivirus-free cells died. Cas9 expression and functionality were confirmed. CRISPR knockout utilized two different sgRNAs delivered to Cas9-expressing cells. Cells in 6-well plates were infected with virus in 8 μg/ml Polyacrylamide for 2 days, treated with 2 μg/ml Puromycin for 4 days, and further proliferated for analysis. Knockout efficiency of edited cell lines was verified through Western blot. The sgRNA sequences used for CRISPR-Cas9 knockout cell line generation were listed in Supplementary Table S4. Lentivirus was produced by transfecting HEK293T cells with the target plasmid and packaging plasmids pSPAX2 and pMD2G at a ratio of 0.8:0.4:0.2. Transfection was carried out using polyethyleneimine hydrochloride reagent (catalog: No. 24885–2, PEI). Virus supernatant was collected 48 h post-transfection, filtered through a 0.45 μm filter, and stored at −80°C for the generation and verification of knockout cell lines.

Flow cytometry

The cells underwent trypsin digestion and centrifugation. A single wash with FACS Buffer was performed. Flow cytometry antibodies were prepared at a dilution ratio of 1:100. The cells were resuspended, stained on ice in the dark for 30 min, and washed once with FACS Buffer. Data acquisition was performed using BD FACSVerse (BD Biosciences), and analysis was conducted using FlowJo software (RRID:SCR_008520).

Immunoprecipitation (IP) and Immunoblotting

IP and Immunoblotting were performed as described above (Freed-Pastor et al., 2021). The cells were harvested, washed in cold PBS, and lysed in CoIP lysis buffer (a mixture of 50 mM Tris-CL (pH 7.4), 0.5 % NP-40, 150 mM NaCl, 1 mM EDTA, 10 % glycerophosphate, and protease inhibitor). After 30 min of lysis, the soluble fraction of cell lysate was separated by centrifugation at 12,000 rpm at 4 °C for 15 min. For IP, cell lysates incubated overnight in HA beads (Abmart) or M2 beads (Sigma) to target specific proteins. The beads were boiled after thorough washing. Protein samples were separated by SDS-PAGE gel electrophoresis and analyzed by Western blot. The proteins were transferred to a PVDF membrane, blocked with 5 % milk, incubated with appropriate primary antibodies, washed with PBS containing Tween, and visualized using chemiluminescence imaging with secondary antibodies labeled with HRP (goat anti-rabbit IgG or goat anti-mouse IgG; Biodragon immunotech). The RRIDs of antibodies have been listed in Supplementary Table S4.

Ubiquitination assay

For *in vivo* ubiquitination assay using COIP, cells were transfected with Myc-ubiquitin. The transfected cells were lysed with lysis buffer (a mixture of 10 mM Tris-HCl (pH 8.0) ,150 mM NaCl, 2 %SDS), and shook for 5 min, boiled at 100°C for 15 min. The boiled sample was then added to dilution buffer (a mixture of 10 mM Tris-HCl (pH 8.0) ,150 mM NaCl, 2 mM EDTA, 1 %Triton), and sonicated using an ultrasonic crusher. After sonication, the sample was centrifuged at

12,000 rpm at 4°C for 30 min. Corresponding beads were prepared, washed with dilution buffer, and centrifuged three times at 4°C and 6000 rpm. The prepared beads were added to the sample and incubated overnight on a rotator at 4°C. Wash buffer (a mixture of 10 mM Tris-HCl (pH 8.0,1 M NaCl, 1 mM EDTA, 1 %NP-40) was used for three washes. After removing the supernatant, loading buffer was added to each sample, mixed, and stored at −20°C.

Real-time quantitative PCR

Total RNA was extracted from various cells with TriZol RNA preparation kit (sigma). After quantification with Nanodrop 1000 spectrophotometer (Thermo Scientific), 1 μg of total RNA was reverse transcribed into complementary DNA with Rever TraAce qPCR RT kit (TOYOBO). Quantitative PCR was performed with SYBR Green Real-time PCR Master Mix (TOYOBO)) and quantitative PCR was performed with Step One Real-time PCR System (Applied Biosystems). The primers for real-time PCR are shown in Supplementary Table S5.

In vivo tumorigenesis construction and treatment

CCNC-knockout MB49 cells (1×10^6/100 μL/ mouse) were inoculated into the right flank of wild-type male C57BL/6 mice or nude mice. Body weight and tumor size changes were monitored every other day after subcutaneous tumor formation. Tumor volume was calculated using the formula: 0.5 * length * width^2. On the 13th day of tumor growth, two groups of tumor-bearing mice (sgCcnc and sgNC) were treated with TIGIT (200ug/mouse, once every 3 days, 5 times total), while the other two groups received IgG as a control. For combination treatments, anti-mouse PD-1 (100ug/mouse, once every 3 days, 5 times total) or PBS combined with PBS or TIGIT (200ug/mouse, once every 3 days, 5 times total) were given intraperitoneally on day 10 after tumor cell inoculation. The animal study was conducted with approval from the Animal Use and Protection Committee of Shanghai Tenth People's Hospital, Tongji University.

Tumor cell dissociation and analysis

A single cell suspension was prepared from the MB49 tumor tissues using tumor lysis buffer containing collagenase IV (1 mg/ml; Yeasen Biotechnology) and DNase I (10 U/ml; Sigma) in serum-free DMEM medium (Wisent Bio Products). Prior to staining for flow cytometry, the tumor cell suspension was washed with FACS buffer, which consisted of 2 % FBS in PBS. Specific markers were labeled using anti-mouse antibodies obtained from Biolegend. The cells were incubated with the antibodies in the dark at 4°C for 30 min. All samples were acquired using BD FACSVerse (BD Biosciences) and analyzed with FlowJo software.

RNA sequencing analysis

Total RNA was extracted from T24 cells of CCNC knockout group and control group. RNA-seq was performed using Illumina HiSeq 2500 (Shanghai OE biotechnology co., ltd.). STAR aligner v2.5 was used to compare the retrieved data with the UCSC human genome (hg19), and feature counting software was used to quantify all hits. Then, RNA-seq data were analyzed by using "DESeq2" and "ClusterProfiler" software. A value with a fold change of 1.35 and an adjusted p value of 0.05 is used as the cut-off value.

In vitro cell growth and viability assays

Cell proliferation was assessed by the Cell Counting Kit-8 (CCK8) assay and cell growth was assessed by colony formation assay as described previously (Mao et al., 2021).

In vitro cell killing evaluation

Flow Cytometry Assay

Tumor cells were washed with PBS and trypsinized, then labeled with CFSE dye (1:2000) in the dark at 37°C for 30 min. After centrifugation at 1000 rpm for 5 min, cells were washed with PBS and resuspended in culture medium at 4×10^5 cells/ml. A total of 0.5 ml of tumor cells was plated per well in 24-well plates. Effector cells (NK92 cells or activated mouse T cells) were added at the indicated effector-to-target (E:T) ratios (NK92 cells, 2:1; T cells, 5:1) in 0.5 ml per well. Plates were centrifuged at 1200 rpm for 5 min and incubated for 16 h at 37°C. After incubation, cells were harvested, stained with Live/Dead dye (1:2000 in cold PBS) for 20 min at 4°C in the dark, washed with PBS, and analyzed by flow cytometry.

Lactate Dehydrogenase (LDH) Release Assay

Tumor cells and effector cells (NK92 or activated T cells) were adjusted to 2×10^5 cells/ml and 1×10^6 cells/ml, respectively. A total of 50 μL tumor cells and 50 μL effector cells were co-cultured in a 96-well round-bottom plate at the indicated E:T ratios (NK92, 5:1; T cells, 5:1). After centrifugation at 250 × g for 4 min, cells were incubated for 18 h at 37°C in 5 % CO_2. At the end of incubation, 10 μL of lysis buffer was added to each well and incubated for 1 h at 37°C, followed by centrifugation at 250 × g for 4 min. A 50 μL aliquot of supernatant was mixed with an equal volume of assay buffer and incubated in the dark at room temperature for 15–20 min. Absorbance was measured at 492 nm using a microplate reader. The specific cytotoxicity was calculated using the formula: [(OD experimental group - OD total natural release) / (OD maximum release group - OD total natural release)] × 100 %.

Immunohistochemical (IHC) analysis

The tissues were fixed in 4 % paraformaldehyde (PFA), embedded in paraffin blocks, and processed for immunohistochemistry. Tissue sections were incubated overnight with antibodies at 4°C. Biotinylated goat anti-rabbit IgG and streptavidin-horseradish peroxidase were used for detection. Tissue staining was performed using diaminobenzidine-H_2O_2 and hematoxylin.

Bladder cancer tissue arrays were used in this study. A bladder cancer tissue chip was stained with CCNC and CD155 antibodies, and the correlation between CCNC and CD155 expression was analyzed. Immunohistochemical staining was evaluated by an independent pathologist. Staining intensity (0–3) and the percentage of positive tumor cells (0–3) were scored separately. The overall immunoreactivity score was calculated by multiplying the intensity score by the percentage score, resulting in a total score ranging from 0 to 9. Samples were categorized as low (0–3) or high (4–9) based on the overall score.

Bioinformatics analysis

The Clinical Information House (https://www.aclbi.com) obtained tumor RNAseq data (level 3) and clinical information from the Cancer Genome Map (TCGA) database (https://portal.gdc.com). Statistical analysis was performed using R software v4.0.3. The rank sum test was used to detect differences between data groups, with a significance level of $p < 0.05$. Univariate Cox regression analysis and forest plots were generated using the "forest plot" R package to display p-values, HR, and 95 % CI.

RNA-seq expression data from 9736 tumor samples and 8587 normal samples, including TCGA and GTEx projects, were obtained from GEPIA 2 (http://gepia2.cancer-pku.cn). We analyzed the expression patterns of FBXO11, CCNC, and CD155 across different tumor types, assessed correlations between these genes, and explored their associations with immune cell infiltration using the platform's correlation and immune infiltration analysis modules.

LISA (http://lisa.cistrome.org) was used to predict transcription factors and chromatin regulators potentially responsible for the

differential expression of FBXO11, CCNC, and CD155 based on DNase-seq and H3K27ac ChIP-seq datasets.

JASPAR (https://jaspar.genereg.net) provided transcription factor binding motifs, which were used to identify potential TF binding sites in the promoter regions of the target genes.

UbiBrowser (http://ubibrowser.ncpsb.org/) was employed to predict and visualize interactions between ubiquitin ligases and substrates, helping to identify E3 ligases that may regulate FBXO11, CCNC, or CD155.

Differential gene expression between normal, tumor, and metastatic tissues was further validated using TNMplot (https://tnmplot.com).

Finally, the prognostic significance of FBXO11, CCNC, and CD155 expression was evaluated using Kaplan-Meier Plotter (http://kmplot.com), which integrates mRNA, miRNA, and protein expression data from over 30,000 samples across 21 tumor types.

Quantification and statistical analysis

Statistical analyses and data visualization were performed using GraphPad Prism 9 software (PRISM, RRID:SCR_005375 and GraphPad Prism, RRID:SCR_002798). Data are presented as mean±standard deviation (SD) from at least three independent experiments unless otherwise stated. For comparisons between two groups, an unpaired two-tailed Student's *t*-test was applied. For comparisons involving more than two groups, one-way or two-way ANOVA followed by appropriate post-hoc multiple comparison tests (e.g., Tukey's or Bonferroni's test) was used, as indicated in figure legends. For analyses involving multiple hypothesis testing, such as CRISPR screen data, the Benjamini-Hochberg method was applied to control the false discovery rate. *P*-values < 0.05 were considered statistically significant. The following significance thresholds were used throughout the study: $^{*}P < 0.05$, $^{**}P < 0.01$, $^{***}P < 0.001$, $^{****}P < 0.0001$. "NS" denotes not significant ($P \geq 0.05$). The specific statistical test used and the exact *P*-value or threshold are indicated in each figure legend.

Materials availability

All unique reagents generated in this study are available from the lead contact with a completed Materials Transfer Agreement.

CRediT authorship contribution statement

Dongdong Wang: Software, Formal analysis. **Chengyuan Dong:** Validation, Software, Data curation. **Zezhi Shan:** Visualization. **Yadong Guo:** Writing – review & editing, Writing – original draft, Software, Methodology, Formal analysis, Data curation. **Shiyu Mao:** Writing – review & editing, Writing – original draft, Visualization, Validation, Methodology, Conceptualization. **Qi Wu:** Formal analysis. **Tingting Niu:** Validation. **Xiao Tan:** Project administration. **Zening Zheng:** Visualization. **Linjun Weng:** Software. **Xinbo Wang:** Software. **Lan Fang:** Writing – review & editing, Visualization, Supervision, Resources, Project administration, Funding acquisition, Formal analysis, Data curation, Conceptualization. **Yaxu Li:** Methodology. **Yanrong Yang:** Investigation. **Xudong Yao:** Writing – review & editing, Project administration, Funding acquisition, Data curation, Conceptualization. **Bing Shen:** Writing – review & editing, Resources, Project administration, Conceptualization. **Jiali Jin:** Supervision. **Yaohui Gao:** Resources. **Xin Ge:** Validation, Resources, Conceptualization. **Ping Wang:** Resources, Conceptualization.

Declaration of Competing Interest

The authors declare the following financial interests/personal relationships which may be considered as potential competing interests: Fang Lan reports financial support was provided by the National Key Research and Development Program of China and by grants from the National Natural Science Foundation of China. Yao Xudong reports financial support was provided by the Experimental Animal Fund of the Shanghai Science and Technology Commission. Mao Shiyu reports financial support was provided by the Tongji University Medicine-X Interdisciplinary Research Initiative. Guo Yadong reports financial support was provided by the Cultivation Grant for Clinical and Basic Integration Research of Shanghai Tenth People's Hospital. If there are other authors, they declare that they have no known competing financial interests or personal relationships that could have appeared to influence the work reported in this paper.

Acknowledgement

We thank Dr. Gang Wang for providing guidance to analysis of CCNC functional mechanisms. We thank Dr. Xiaoqing Zhang for sharing the NK92 cells. We thank Dr. Wenhui Zhang for performing the supplementary experiments in response to the reviewer's comments, which validated that CDK8-mediated phosphorylation, protein stability, and nuclear localization of FOSL2 were not affected by CCNC knockout. This study was supported by the National Key Research and Development Program of China (2022YFC3401500, 2020YFA0803201, 2022YFB3804504), the Grants from the National Natural Science Foundation of China (82341028, 82203505, 82203520, 82203367, 82101838), Tongji University Medicine-X Interdisciplinary Research Initiative (2025–0553–18–02), Cultivation grant for clinical and basic integration research of Shanghai Tenth People's Hospital (SYYYRH-2025–034) ,the Experimental Animal Fund of Shanghai Science and Technology Commission (22140903800).

Appendix A. Supporting information

Supplementary data associated with this article can be found in the online version at doi:10.1016/j.drup.2025.101318.

Data availability statement

RNA-seq data generated in this study are available at NCBI GEO database with the accession number GSE278902. Any additional information required to re-analyze the data reported in this paper is available from the lead contact upon request.

References

Chen, D.S., Mellman, I., 2017. Elements of cancer immunity and the cancer-immune set point. Nature 541 (7637), 321–330.
Kubli, S.P., Berger, T., Araujo, D.V., Siu, L.L., Mak, T.W., 2021. Beyond immune checkpoint blockade: emerging immunological strategies. Nat. Rev. Drug Discov. 20 (12), 899–919.
Freed-Pastor, W.A., Lambert, L.J., Ely, Z.A., Pattada, N.B., Bhutkar, A., Eng, G., et al., 2021. The CD155/TIGIT axis promotes and maintains immune evasion in neoantigen-expressing pancreatic cancer. Cancer Cell 39 (10), 1342–1360 e1314.
Ribas, A., Wolchok, J.D., 2018. Cancer immunotherapy using checkpoint blockade. Science (New York NY) 359 (6382), 1350–1355.
Guan, X., Hu, R., Choi, Y., Srivats, S., Nabet, B.Y., Silva, J., et al., 2024. Anti-TIGIT antibody improves PD-L1 blockade through myeloid and T(reg) cells. Nature 627 (8004), 646–655.
Sharma, P., Goswami, S., Raychaudhuri, D., Siddiqui, B.A., Singh, P., Nagarajan, A., et al., 2023. Immune checkpoint therapy-current perspectives and future directions. Cell 186 (8), 1652–1669.
Wang, Z., Wang, W., Leung, C.H., 2024. Strategies for Developing Cancer Theranostics Approaches. Recent Pat. Anticancer Drug Discov. 19 (2), 130–136.
Gao, J., Zheng, Q., Xin, N., Wang, W., Zhao, C., 2017. CD155, an onco-immunologic molecule in human tumors. Cancer Sci. 108 (10), 1934–1938.
Pende, D., Castriconi, R., Romagnani, P., Spaggiari, G.M., Marcenaro, S., Dondero, A., et al., 2006. Expression of the DNAM-1 ligands, Nectin-2 (CD112) and poliovirus receptor (CD155), on dendritic cells: relevance for natural killer-dendritic cell interaction. Blood 107 (5), 2030–2036.
O'Donnell, J.S., Madore, J., Li, X.Y., Smyth, M.J., 2020. Tumor intrinsic and extrinsic immune functions of CD155. Semin Cancer Biol. 65, 189–196.
Braun, M., Aguilera, A.R., Sundarrajan, A., Corvino, D., Stannard, K., Krumeich, S., et al., 2020a. CD155 on Tumor Cells Drives Resistance to Immunotherapy by Inducing the Degradation of the Activating Receptor CD226 in CD8(+) T Cells. Immunity 53 (4), 805–823 e815.

Shibuya, A., Campbell, D., Hannum, C., Yssel, H., Franz-Bacon, K., McClanahan, T., et al., 1996. DNAM-1, a novel adhesion molecule involved in the cytolytic function of T lymphocytes. Immunity 4 (6), 573–581.
Martinet, L., Smyth, M.J., 2015. Balancing natural killer cell activation through paired receptors. Nat. Rev. Immunol. 15 (4), 243–254.
Ding, S., Zhang, T., Lei, Y., Liu, C., Liu, Z., Fu, R., 2024. The role of TIM3(+) NK and TIM3(-) NK cells in the immune pathogenesis of severe aplastic anemia. J. Transl. Int Med 12 (1), 96–105.
Banta, K.L., Xu, X., Chitre, A.S., Au-Yeung, A., Takahashi, C., O'Gorman, W.E., et al., 2022a. Mechanistic convergence of the TIGIT and PD-1 inhibitory pathways necessitates co-blockade to optimize anti-tumor CD8(+) T cell responses. Immunity 55 (3), 512–526 e519.
Yang, C., Geng, H., Yang, X., Ji, S., Liu, Z., Feng, H., et al., 2024. Targeting the immune privilege of tumor-initiating cells to enhance cancer immunotherapy. Cancer Cell 42 (12), 2064–2081 e2019.
Chu, X., Tian, W., Wang, Z., Zhang, J., Zhou, R., 2023. Co-inhibition of TIGIT and PD-1/PD-L1 in cancer immunotherapy: mechanisms and clinical trials. Mol. Cancer 22 (1), 93.
Cho, B.C., Abreu, D.R., Hussein, M., Cobo, M., Patel, A.J., Secen, N., et al., 2022. Tiragolumab plus atezolizumab versus placebo plus atezolizumab as a first-line treatment for PD-L1-selected non-small-cell lung cancer (CITYSCAPE): primary and follow-up analyses of a randomised, double-blind, phase 2 study. Lancet Oncol. 23 (6), 781–792.
Briukhovetska, D., Suarez-Gosalvez, J., Voigt, C., Markota, A., Giannou, A.D., Schübel, M., et al., 2023. T cell-derived interleukin-22 drives the expression of CD155 by cancer cells to suppress NK cell function and promote metastasis. Immunity 56 (1), 143–161 e111.
Nakanishi, T., Yoneshima, Y., Okamura, K., Yanagihara, T., Hashisako, M., Iwasaki, T., et al., 2023. MicroRNA-326 negatively regulates CD155 expression in lung adenocarcinoma. Cancer Sci. 114 (10), 4101–4113.
Dersh, D., Phelan, J.D., Gumina, M.E., Wang, B., Arbuckle, J.H., Holly, J., et al., 2021. Genome-wide screens identify lineage- and tumor-specific genes modulating MHC-I- and MHC-II-restricted immunosurveillance of human lymphomas. Immunity 54 (1), 116–131 e110.
Burr, M.L., Sparbier, C.E., Chan, K.L., Chan, Y.C., Kersbergen, A., Lam, E.Y.N., et al., 2019. An evolutionarily conserved function of polycomb silences the MHC Class I antigen presentation pathway and enables immune evasion in cancer. Cancer Cell 36 (4), 385–401 e388.
Chen, X., Lu, Q., Zhou, H., Liu, J., Nadorp, B., Lasry, A., et al., 2023. A membrane-associated MHC-I inhibitory axis for cancer immune evasion. Cell 186 (18), 3903–3920 e3921.
Li, H., Lahti, J.M., Valentine, M., Saito, M., Reed, S.I., Look, A.T., et al., 1996. Molecular cloning and chromosomal localization of the human cyclin C (CCNC) and cyclin E (CCNE) genes: deletion of the CCNC gene in human tumors. Genomics 32 (2), 253–259.
Freitas, K.A., Belk, J.A., Sotillo, E., Quinn, P.J., Ramello, M.C., Malipatlolla, M., et al., 2022. Enhanced T cell effector activity by targeting the Mediator kinase module. Science (New York NY) 378 (6620), eabn5647.
Chen, X., Yin, X., Li, J., Wu, Z., Qi, Y., Wang, X., et al., 2021a. Structures of the human Mediator and Mediator-bound preinitiation complex. Science 372 (6546).
Koschubs, T., Lorenzen, K., Baumli, S., Sandström, S., Heck, A.J., Cramer, P., 2010. Preparation and topology of the Mediator middle module. Nucleic Acids Res. 38 (10), 3186–3195.
Ismail, I.H., Gagné, J.P., Genois, M.M., Strickfaden, H., McDonald, D., Xu, Z., et al., 2015. The RNF138 E3 ligase displaces Ku to promote DNA end resection and regulate DNA repair pathway choice. Nat. Cell Biol. 17 (11), 1446–1457.
Komatsu, M., Inada, T., Noda, N.N., 2024. The UFM1 system: working principles, cellular functions, and pathophysiology. Mol. Cell 84 (1), 156–169.
Tahara-Hanaoka, S., Shibuya, K., Kai, H., Miyamoto, A., Morikawa, Y., Ohkochi, N., et al., 2006. Tumor rejection by the poliovirus receptor family ligands of the DNAM-1 (CD226) receptor. Blood 107 (4), 1491–1496.
Banta, K.L., Xu, X., Chitre, A.S., Au-Yeung, A., Takahashi, C., O'Gorman, W.E., et al., 2022b. Mechanistic convergence of the TIGIT and PD-1 inhibitory pathways necessitates co-blockade to optimize anti-tumor CD8(+) T cell responses. Immunity 55 (3), 512–526 e519.
Fang, S., Jin, X., Zhou, C., Gong, Z., 2022. Cyclin C: a new responser for chemosensitivity in cancer. Clin. Transl. Med 12 (4), e833.
Tang, M., Pei, G., Su, D., Wang, C., Feng, X., Srivastava, M., et al., 2021. Genome-wide CRISPR screens reveal cyclin C as synthetic survival target of BRCA2. Nucleic Acids Res 49 (13), 7476–7491.
Braun, M., Aguilera, A.R., Sundarrajan, A., Corvino, D., Stannard, K., Krumeich, S., et al., 2020b. CD155 on tumor cells drives resistance to immunotherapy by inducing the degradation of the activating receptor CD226 in CD8(+) T cells. Immunity 53 (4), 805–823 e815.
Lepletier, A., Madore, J., O'Donnell, J.S., Johnston, R.L., Li, X.Y., McDonald, E., et al., 2020. Tumor CD155 expression is associated with resistance to anti-PD1 immunotherapy in metastatic melanoma. Clin. Cancer Res 26 (14), 3671–3681.
Li, N., Fassl, A., Chick, J., Inuzuka, H., Li, X., Mansour, M.R., et al., 2014. Cyclin C is a haploinsufficient tumour suppressor. Nat. Cell Biol. 16 (11), 1080–1091.
Lloyd, R.L., Urban, V., Munoz-Martinez, F., Ayestaran, I., Thomas, J.C., de Renty, C., et al., 2021. Loss of Cyclin C or CDK8 provides ATR inhibitor resistance by suppressing transcription-associated replication stress. Nucleic Acids Res 49 (15), 8665–8683.
Broude, E.V., Gyorffy, B., Chumanevich, A.A., Chen, M., McDermott, M.S., Shtutman, M., et al., 2015. Expression of CDK8 and CDK8-interacting Genes as Potential Biomarkers in Breast Cancer. Curr. Cancer Drug Targets 15 (8), 739–749.
Rengachari, S., Schilbach, S., Aibara, S., Dienemann, C., Cramer, P., 2021. Structure of the human Mediator-RNA polymerase II pre-initiation complex. Nature 594 (7861), 129–133.
Xu, W., Ji, J.Y., 2011. Dysregulation of CDK8 and Cyclin C in tumorigenesis. J. Genet Genom. 38 (10), 439–452.
Hirota, T., Irie, K., Okamoto, R., Ikeda, W., Takai, Y., 2005. Transcriptional activation of the mouse Necl-5/Tage4/PVR/CD155 gene by fibroblast growth factor or oncogenic Ras through the Raf-MEK-ERK-AP-1 pathway. Oncogene 24 (13), 2229–2235.
Chen, G.L., Li, R., Chen, X.X., Wang, J., Cao, S., Song, R., et al., 2021b. Fra-2/AP-1 regulates melanoma cell metastasis by downregulating Fam212b. Cell Death Differ. 28 (4), 1364–1378.
Bejjani, F., Tolza, C., Boulanger, M., Downes, D., Romero, R., Maqbool, M.A., et al., 2021. Fra-1 regulates its target genes via binding to remote enhancers without exerting major control on chromatin architecture in triple negative breast cancers. Nucleic Acids Res 49 (5), 2488–2508.
Bian, Z., Zhou, M., Cui, K., Yang, F., Cao, Y., Sun, S., et al., 2021. SNHG17 promotes colorectal tumorigenesis and metastasis via regulating Trim23-PES1 axis and miR-339-5p-FOSL2-SNHG17 positive feedback loop. J. Exp. Clin. Cancer Res 40 (1), 360.
Higuchi, T., Nakayama, T., Arao, T., Nishio, K., Yoshie, O., 2013. SOX4 is a direct target gene of FRA-2 and induces expression of HDAC8 in adult T-cell leukemia/lymphoma. Blood 121 (18), 3640–3649.
Yu, M., Peng, Z., Qin, M., Liu, Y., Wang, J., Zhang, C., et al., 2021. Interferon-gamma induces tumor resistance to anti-PD-1 immunotherapy by promoting YAP phase separation. Mol. Cell 81 (6), 1216–1230 e1219.
Jiang, C., Trudeau, S.J., Cheong, T.C., Guo, R., Teng, M., Wang, L.W., et al., 2019. CRISPR/Cas9 screens reveal multiple layers of B cell CD40 regulation. Cell Rep. 28 (5), 1307–1322 e1308.
Chan, K.L., Gomez, J., Cardinez, C., Kumari, N., Sparbier, C.E., Lam, E.Y.N., et al., 2022. Inhibition of the CtBP complex and FBXO11 enhances MHC class II expression and anti-cancer immune responses. Cancer Cell 40 (10), 1190–1206 e1199.
Gose, T., Rasouli, A., Dehghani-Ghahnaviyeh, S., Wen, P.C., Wang, Y., Lynch, J., et al., 2024. Tumor-acquired somatic mutation affects conformation to abolish ABCG2-mediated drug resistance. Drug Resist Updat 73, 101066.
Zhang, X., Tan, Y., Li, T., Tan, D., Fu, B., Yang, M., et al., 2024. Intercellular adhesion molecule-1 suppresses TMZ chemosensitivity in acquired TMZ-resistant gliomas by increasing assembly of ABCB1 on the membrane. Drug Resist Updat 76, 101112.
Yang, C., Jin, J., Yang, Y., Sun, H., Wu, L., Shen, M., et al., 2022. Androgen receptor-mediated CD8(+) T cell stemness programs drive sex differences in antitumor immunity. Immunity 55 (7), 1268–1283 e1269.
Hargrove-Wiley, E., Fingleton, B., 2023. Sex hormones in breast cancer immunity. Cancer Res 83 (1), 12–19.
Alspach, E., 2023. So grateful for My X: sex chromosomes drive differences in glioblastoma immunity. Cancer Discov. 13 (9), 1966–1968.
Tao, X., Wang, Y., Xiang, B., Hu, D., Xiong, W., Liao, W., et al., 2025. Sex bias in tumor immunity: insights from immune cells. Theranostics 15 (11), 5045–5072.
Mao, S., Zhang, W., Yang, F., Guo, Y., Wang, H., Wu, Y., et al., 2021. Hsa_circ_0004296 inhibits metastasis of prostate cancer by interacting with EIF4A3 to prevent nuclear export of ETS1 mRNA. J. Exp. Clin. Cancer Res 40 (1), 336.